JOURNAL OF MATERIALS SCIENCE 20 (1985) 4657–4680

Sliding friction and wear of structural ceramics

Part 1 *Room temperature behaviour*

J. BREZNAK, E. BREVAL, N. H. MACMILLAN
Materials Research Laboratory, Pennsylvania State University, University Park, Pennsylvania 16802, USA

A study has been made of the unlubricated sliding friction and wear behaviour of various like and unlike combinations of four materials – sintered α-SiC, graphitized SiC, siliconized SiC and a Y_2O_3-stabilized ZrO_2 – in air at room temperature under dynamic conditions approximating the motion of a piston in the cylinder of an idling automotive engine. The steady state friction coefficient μ_f is largely independent of the initial surface finish, but is in all cases unacceptably high ($0.25 \leqslant \mu_f \leqslant 0.50$) for engine applications. When the running-in process involves smoothing of the wear surfaces, the coefficient of friction decreases asymptotically towards its steady state value; and when running-in involves roughening, this coefficient usually increases asymptotically as the wear surfaces develop their steady state topographies. Friction couples containing siliconized SiC were the only exceptions to this pattern of behaviour. In every case the high steady state friction is accompanied by considerable wear. The results suggest that ceramic components will not be used unlubricated in reciprocating situations.

1. Introduction

The prospect of reducing fuel consumption by raising engine operating temperature and thereby increasing thermodynamic efficiency has recently led to great interest in using ceramic materials in the construction of both reciprocating and turbine engines [1–5]. In practice, however, the hoped-for economy will only be realized if the friction losses can be kept to an acceptably low level. To do this will be no mean feat because none of the lubricants used in present generation engines can long survive at the temperatures at which ceramic engines become attractive. It is therefore pertinent to investigate the friction and wear properties of the principal structural ceramics – Al_2O_3, partially stabilized ZrO_2, SiC, Si_3N_4 and the SiAlON's – as functions of temperature in both the lubricated and the unlubricated state. The present paper starts down this road by investigating the unlubricated sliding friction and wear behaviour of three forms of SiC and a Y_2O_3-stabilized ZrO_2 in reciprocating motion at ambient temperature.

The current understanding of friction derives primarily from the work of the Cambridge school led by Bowden and Tabor [6, 7]. This view emphasizes that the force of attraction between two surfaces has two components: (1) a weak, long-range van der Waals interaction, which can act over a significant fraction of the nominal area of contact; and (2) a potentially much stronger short-range interaction, which may be ionic, covalent or metallic, depending on the chemistry of the surfaces involved. This stronger component acts only over the true area of contact, i.e., that small fraction of the nominal area over which asperities on the opposing surfaces close to within about one atomic diameter. Hence, it is argued that friction between

0022–2461/85 $03.00 + .12

nominally flat surfaces arises primarily from the making and breaking of contacts between opposing asperities and from the deformation of the asperities that accompanies these processes. The picture gets more complex when one of the opposing surfaces has a sufficiently small radius of curvature and/or is sufficiently heavily loaded that it penetrates into the other to a depth greater than the characteristic dimensions of the asperities on either, because there is then an additional "ploughing" contribution to the friction arising from plastic flow and/or fracture of the material underlying the asperities. In the case of well-polished macroscopic engine components, which typically have root mean square surface finishes in the 0.25 to 2.5 μm (1 to 10 micro-inch range), this latter term is unlikely to be important. Consequently, it was regarded as important in this study to adopt a contact geometry involving two large flat surfaces rather than one involving a "sharp" stylus and a flat surface.

Several factors affect the behaviour of asperities at a sliding interface. One is the chemical composition of the surfaces. This dictates the nature of the chemical bonds that form in the regions of true contact and hence determines the magnitudes of the forces exerted on the asperities. Relatively little is known about the adhesion of ceramics [8], making it difficult to infer the behaviour of one friction couple from observations of the behaviour of another. This is another reason for not using a diamond stylus to simulate ceramic engine wear. In so far as chemical composition also determines the elastic constants, glide elements, cleavage planes, etc. of the materials involved in the contact, this factor further affects the response of the asperities to the forces applied to them. It also provides a third reason for avoiding the use of diamond styli to simulate engine operation.

A second important determinant of asperity behaviour is the method of surface preparation. This determines not only the sizes, shapes and spatial distribution of the asperities, but also their defect content, which latter in turn affects their response to stress. For this reason, the present experiments include specimens prepared in several different ways. It is also worth noting here that it is not safe to infer either the defect content or the elastic–plastic response of surface asperities from the structural characteristics and the behaviour of the same solid in bulk form.

The remaining important factor influencing the behaviour of asperities in contact phenomena is the environment in which the contact takes place. This can have at least three quite different influences. In sufficient quantity and under sufficient pressure, it can act as a hydrodynamic lubricant by holding the surfaces far enough apart to prevent bonding. Alternatively, because chemical bonding processes take place only over distances of atomic dimensions, adsorption of even a monolayer of some environmental species can profoundly affect such processes. In particular, the adsorbate may act as a boundary lubricant by reducing bonding. Finally, the environment may affect the near-surface flow and/or fracture properties of either or both of the solids in contact to some characteristic depth via a variety of mechanisms (liquid metal embrittlement, hydrogen embrittlement, complex-ion embrittlement, chemo-mechanical (Rebinder) effects, etc. [9, 10]).

In the case of the ceramic engine, the operating environment cannot yet be fully defined. It will certainly contain a mixture of air and either gasoline or kerosene, plus the products of combustion of such a mixture; but what other substances will be needed as fuel additives, lubricants, lubricant additives, etc. remains to be established. The issue is avoided in the present paper which, as the first of a series, seeks only to elucidate the "baseline" friction and wear behaviour under ambient conditions; but it will have to be addressed in succeeding papers of the series. It is relevant to note that, when the sticking coefficient is unity, the time required to form a monolayer of adsorbate in air at ambient conditions is $\lesssim 1\mu$sec [11]. This time is short compared to the time between successive revolutions of either reciprocating or turbine engines.

2. Experimental methods

Fig. 1 shows the friction apparatus configured for room temperature operation. Motive power is supplied by a 0.125 hp direct current electric motor which is continuously adjustable in speed from 0 to 1725 rpm. The motor is mounted on a large (110 cm $\times$ 45 cm) aluminium base plate which sits on anti-vibration mounts set into a concrete floor. It is connected via a 3:2 belt drive and an eccentrically mounted crank to a stainless steel upper (moving) specimen support tube carried in two collinear bearings. Maximum

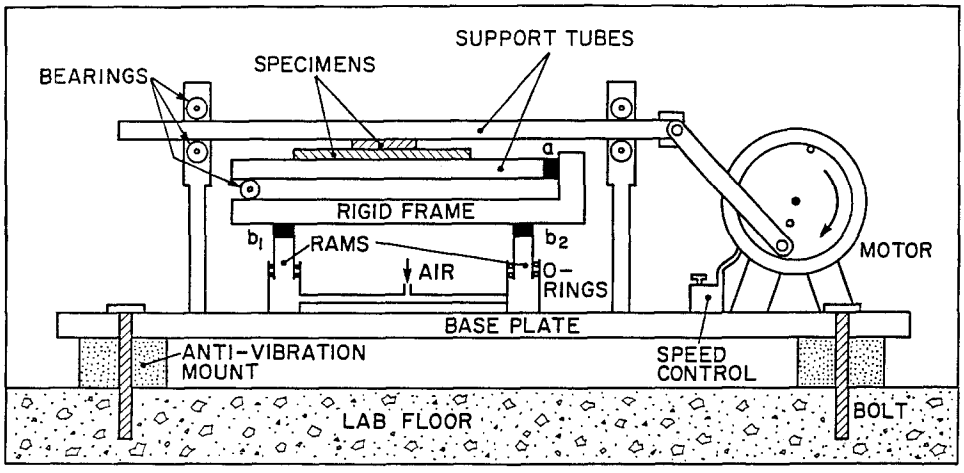

Figure 1 Schematic diagram of the friction apparatus.

speed is 2588 rpm; and the stroke can be adjusted from 5 to 12.5 cm by varying the eccentricity of the crank. The upper specimen is a rectangular parallelipiped 5 cm long, 2.5 cm wide and 1 cm thick. It is rigidly fastened to the underside of the upper support tube by a special clamp, Fig. 2. The lower (stationary) specimen is a 15 cm × 3 cm × 1 cm rectangular parallelipiped and is fastened in the same fashion to the upper side of the stainless steel lower support tube. This tube is in turn carried by a pneumatically supported rigid frame to which it is fixed at one end via a Kistler Model 9212 quartz piezoelectric force transducer (a). The other end of the support tube rests on a freely running bearing attached to the rigid frame. The pneumatic support for the rigid frame consists of two 2.54 cm diameter piston and cylinder devices connected to a common air supply. Neoprene "O"-rings are used to provide the seals between the pistons and their housings because these allow the pistons sufficient lateral play to ensure optimum mating of the upper and lower specimens across their common interface. Between the pistons and the rigid frame are mounted two other Model 9212 transducers [(b_1) and (b_2)].

The transducer (a) is mounted with its axis parallel to the sliding direction (i.e., horizontally) and coplanar with the sliding interface. Its output goes via a Kistler model 5004 high impedance charge amplifier to one input channel of a dual beam storage oscilloscope. The transducers (b_1) and (b_2) have their axes collinear with the axes of the pneumatic pistons and perpendicular to the sliding interface (i.e., vertical). They are connected in parallel via a similar charge amplifier to the second channel of the oscilloscope. Each transducer/charge amplifier assembly records in both tension and compression and has a time constant which can be varied from ~1 sec to a few hours. In the present work the longest time constant has been used exclusively.

To begin operation, all three transducers are

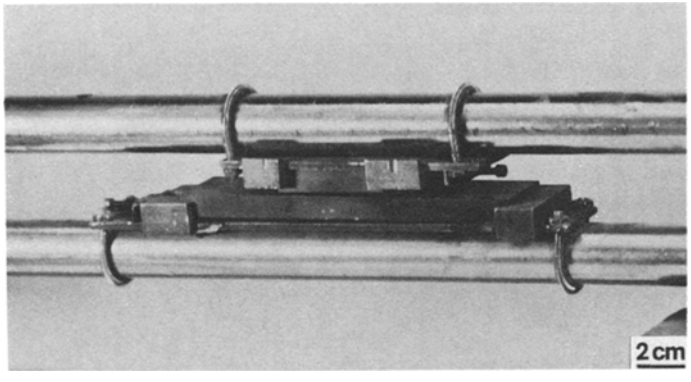

Figure 2 The specimens and the clamps which hold them to their support tubes. The upper support tube moves horizontally and the lower is loaded vertically against it.

first zeroed with the air supply off and no contact between the upper and lower specimens. In the case of transducers (b_1) and (b_2) this compensates for the weight of the rigid frame and the lower specimen and its support tube. The air pressure is then increased to raise the rigid frame and press the specimens together with the requisite normal force, as measured by the transducers (b_1) and (b_2). Finally, the motor is turned on and the upper specimen is caused to slide to and fro over the lower with the requisite speed and stroke. The speed is monitored with a digital tachometer. The friction force F generated by the motion is continously recorded by the transducer (a). The normal force N is also recorded continuously during runs by monitoring the sum of the outputs from transducers (b_1) and (b_2). Hence a continuous record of the coefficient of friction

$$\mu_f = |F|/N$$

can be obtained. For runs lasting several hours the system is periodically stopped, unloaded, re-zeroed and restarted to minimize the effects of the finite time constant.

All of the present experiments with this apparatus were run in air at room temperature (295 to 298 K). The relative humidity varied between 35 and 55%. In each case the sliding motion had a frequency of 10 Hz and a stroke of 7.5 cm, corresponding to an average sliding speed of 1.5 m sec^{-1}, and the pressure in the pneumatic cylinders was maintained constant at a value corresponding to a nominal normal stress (normal force divided by the nominal contact area) of 35 kPa across the sliding interface. These conditions are quite mild compared with those at the piston/cylinder interface in the "adiabatic" diesel engine recently tested by Cummins. This engine, which uses plasma-sprayed coatings of fully stabilized ZrO_2 on its combustion chamber parts, has a 15 cm stroke and develops 170 kW (230 hp) at 35 Hz (2100 rpm) [12]. The average sliding velocity is thus 10.5 m sec^{-1}, and the peak normal stress developed between the piston skirt and the cylinder wall is ~ 2 MPa [13].

Figs. 3a to c show the variation of F (upper trace) and N (lower trace) in the case of diamond lapped and polished sintered α-SiC sliding against itself (see below) after 300, 144 000 and 378 000 cycles of operation, respectively. Such behaviour is typical. It is apparent that vibration

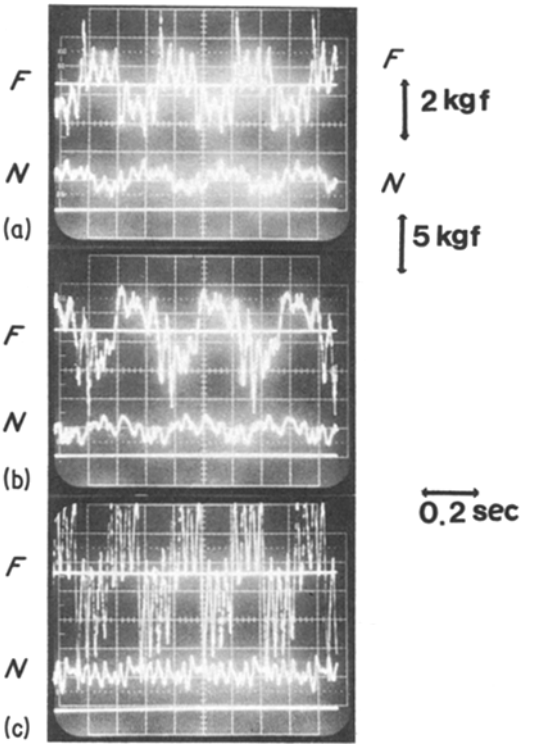

Figure 3 Plots of F (upper trace) and N (lower trace) against time for lapped and polished α-SiC sliding against itself after (a) 300, (b), 144 000 and (c) 378 000 cycles of operation. The zero of the force scale is also indicated for both F and N.

exerts a considerable influence on the variation of F and N during each cycle, and that it does this in a manner which changes little from one cycle to the next but substantially over 10^4 or 10^5 cycles. The values of μ_f reported in this paper were obtained from such plots by averaging $|F|$ and N over three or four successive cycles of operation and finding the ratio $|\bar{F}|/\bar{N}$. A better procedure would be to find $(\overline{|F|/N})$ over a similar number of cycles of operation, but the electronics necessary to do this were not available.

Once the apparatus is set in operation, considerable heat (~ 20 J sec^{-1}) is generated at the sliding interface. In the case of the ZrO_2 material sliding on itself (see below), weak flashes of pale pink light are also emitted at the sliding interface. These are clearly visible to the fully dark-adapted eye when the apparatus is run in a totally blacked-out room. One consequence of the heat generation is that the bulk temperature of the specimens rises over a time of ~ 15 min ($\sim 10^4$ cycles of operation) to 550 to 600 K. The changes in the appearances of the oscilloscope

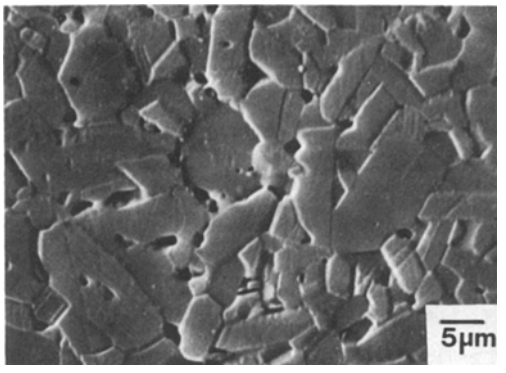

Figure 4 Sintered α-SiC; 5 to 10 μm grain size; ~2 vol % of ~2 μm pores; polished with 1 μm diamond paste on Buehler Microcloth and etched for ~30 sec in a molten 50:50 mixture by weight of KOH and KNO_3.

traces illustrated in Fig. 3 cannot be due to this temperature rise because they persist long after the bulk specimen temperature has stabilized. Rather they appear to arise from changes in the vibrational spectrum of the apparatus which are in turn caused by changes in the nature of the contact at the sliding interface, wear of the bearings carrying the specimen support tubes, etc. A comparison of the outputs from the two normal force transducers (b_1) and (b_2), Fig. 1, reveals that these differ in phase by an angle of ~20° rather than the expected 180°. Physically, this implies that the lower "fixed" specimen is actually moving up and down normal to the sliding interface rather than pitching about an axis lying parallel to this interface and perpendicular to the direction of sliding, i.e., that the effective modulus of the sliding interface and the bearings carrying the upper support tube is lower than the effective modulus of the pneumatic piston and cylinder arrangement. It is important to note that the phenomenon of "piston slap" also produces large variations of similar frequency in the normal force acting across the interface between piston and cylinder during the operation of a reciprocating engine [13].

The surfaces of the specimens were characterized before, during interrruptions in, and after wear tests by optical and scanning electron microscopy and diamond stylus surface profilometry. The profilometer stylus was a square pyramid with an angle of 90° between opposing face normals and a tip radius of ~2.5 μm in the direction of motion and ~7.5 μm perpendicular to this direction. These characteristics necessarily limit the accuracy with which the stylus can trace the micron-scale features of the various surface topographies involved.

3. Experimental materials

Experiments were performed with like and unlike pairs of specimens of four different materials prepared by Sohio Engineered Materials Co. (Niagara Falls, New York 14302): sintered α-SiC, graphitized SiC (C–SiC), siliconized SiC (Si–SiC) and Y_2O_3-stabilized ZrO_2 (PSZ). The phase compositions, some microstructural information, and those mechanical properties generally regarded as indicative of friction and wear behaviour are summarized in Table I. The microstructures are shown in Figs. 4 to 7. Those data indicated by asterisks were provided by Sohio Engineering Materials Co.; the other data were obtained by the present authors.

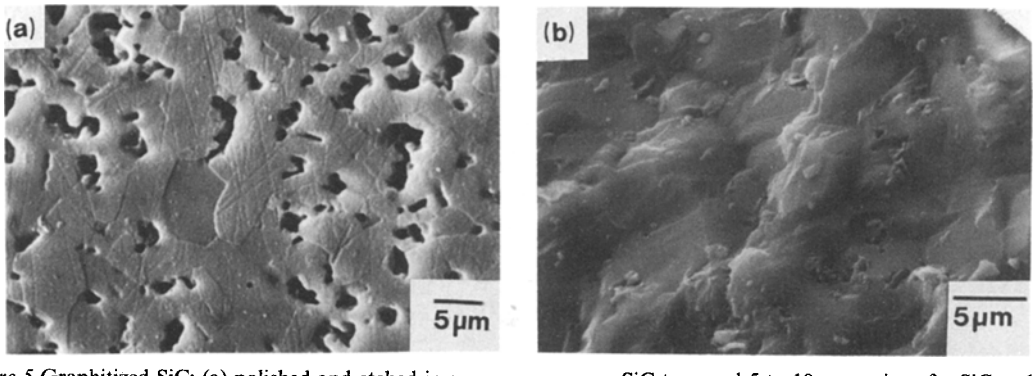

Figure 5 Graphitized SiC: (a) polished and etched in same manner as α-SiC to reveal 5 to 10 μm grains of α-SiC and 5 to 6 vol % of pores and ~2 vol % of graphite inclusions; and (b) fracture surface showing both empty pores and graphite inclusions.

TABLE I Properties of the test materials

Material	α-SiC	C–SiC	Si–SiC	PSZ
Phase composition (wt %)	> 98 α-SiC (6-H, 4-H and 15-R polytypes), 0.5 B_4C + trace graphite*	> 98 α-SiC (6-H, 4-H and 15-R polytypes) + 1–2 graphite	41 Si + 59 α-SiC (6-H, 4-H and 15-R polytypes)*	5 Y_2O_3 + 95 ZrO_2 (tetragonal + trace monoclinic)*
Microstructure	7–10 μm angular equiaxed grains	7–10 μm angular equiaxed SiC grains, containing ~2 vol % of 0.3 to 3 μm graphite inclusions	1–4 μm angular equiaxed SiC grains in Si matrix, average SiC grain size ~2 μm	0.2–1 μm angular equiaxed grains
Porosity (vol %)	~2, closed	5–6, closed	~0	≪1
Pore size (μm)	0.2 to 2	0.3 to 3	–	~1
Density (10^3 kg m^{-3})	3.133	2.988	2.789, 2.830*	5.878
(% theoretical)	97.4	93.6	~100	~100
Young's modulus (GPa)	426, 386*	403, 394*	273, 289*	208, 200*
Poisson's ratio	0.14	0.16	0.20	0.25
Vickers hardness (GPa)	32.4, 24.7*	34.0, 20*	12.8	12.6, 11.8*
Fracture toughness (MPa m$^{1/2}$)	3.41*	3.60*	2.85	4.93*
Work of fracture (J m^{-2})	27.3	32.2	29.8	117

*Data supplied by Sohio Engineered Materials Co.

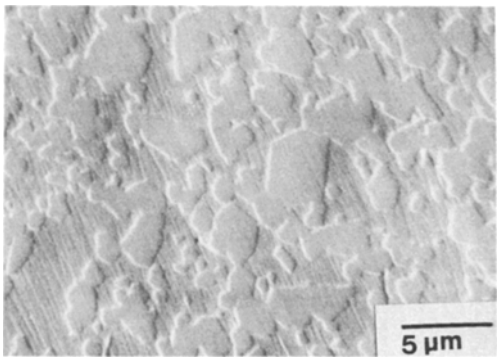

Figure 6 Siliconized SiC polished in the same manner as α-SiC and etched for 10 sec in a mixture of 25 vol % cHF: 25 vol % $cHNO_3$: 50 vol % H_2O to reveal 1 to 4 μm grains of α-SiC in a Si matrix and near-zero porosity.

X-ray diffractometry showed that all three SiC materials contained the same mix of polytypes as is usually found in Acheson-process SiC [14], i.e., a large amount of 6-H and lesser amounts of 4-H and 15-R. Grain size and porosity were studied by ceramography. This revealed that the SiC grain size was considerably finer in the Si–SiC, Fig. 6, than in the α-SiC, Fig. 4, or the C–SiC, Fig. 5. It also revealed that the Si–SiC was essentially theoretically dense and that the α-SiC contained ~2 vol % of 0.2 to 2 μm diameter closed pores. These observations are consistent with the measured densities and the reported phase compositions. In the case of C–SiC, the ceramographic studies did not differentiate clearly between "empty" pores and pores containing graphite, Fig. 5a. From the measured density and the results of quantitative X-ray diffractometry and thermal analysis studies (which both showed the graphite content of C–SiC to be 2 to 3 times that of α-SiC), however, it can be inferred that C–SiC contains ~2 vol % of graphite and 5 to 6 vol % of empty pores. Both the graphite inclusions and the empty pores are isolated and range in size from 0.3 to 3 μm.

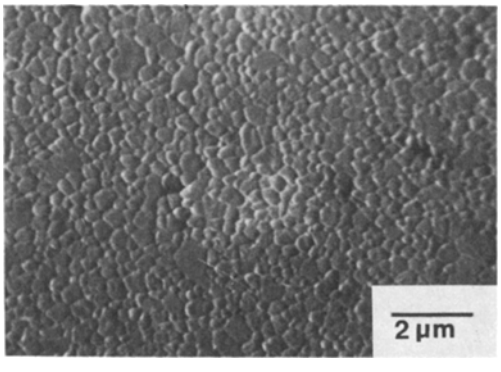

Figure 7 Y_2O_3-stabilized ZrO_2 polished in the same manner as α-SiC and then etched by heating in air at 1673 K for 2 h and air cooling to reveal 0.2 to 1 μm equiaxed angular grains and near-zero porosity. A sample etched for 6 h at the same temperature exhibited the same grain size, demonstrating that the etching procedure did not lead to grain growth.

According to the phase diagram proposed by Scott [15], the PSZ should contain large amounts of the tetragonal phase and small amounts of the cubic phase over the temperature range ~800 to >1800 K; and below ~800 K the tetragonal phase should transform into a eutectoid mixture of the monoclinic and cubic phases to the extent that the kinetics of the transformation permit. The X-ray diffraction studies confirmed the presence of large amounts of the tetragonal phase and small amounts of the monoclinic phase, but provided no clear evidence of the presence of the cubic phase. The ceramographic studies showed the grain size to be 0.2 to 1 μm and the grain shape to be angular and equiaxed, Fig. 7. The porosity was found to be essentially zero, in accord with the density measurements.

Young's modulus and Poisson's ratio were determined ultrasonically, by the standing wave (resonance) technique; the fracture toughness was measured by the indentation technique as promulgated by Evans [16], using a Vickers indenter and loads of 10 to 20 N or 50 N; and the work of fracture was calculated from the measured elastic constants and fracture toughness. The Vickers hardness measurements were made in two load regimes. Those values marked with an asterisk were obtained using a load of 50 N and those without asterisks were measured at loads of 2 to 10 N.

4. Results and discussion

4.1. Sliding behaviour of α-SiC on α-SiC as a function of initial surface finish

Fig. 8 shows the temporal dependence of the coefficient of friction for four differently prepared like pairs of α-SiC specimens. In Case I both specimens were prepared by machine grinding their mating surfaces parallel to the sliding direction with a relatively coarse diamond wheel. The specimens used in Case II were similarly machined with a finer such wheel, and

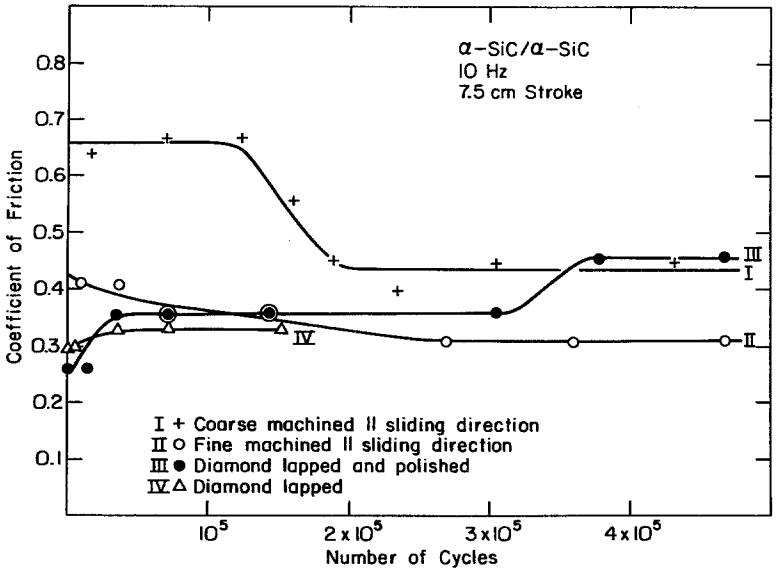

Figure 8 Variation of the coefficient of friction with number of cycles of sliding wear for variously machined α-SiC/α-SiC friction couples.

those used in Cases III and IV were diamond lapped and polished and diamond lapped, respectively, to produce still smoother, non-directional finishes.

Fig. 9 shows profilometer traces made prior to start-up in directions parallel and perpendicular to the sliding direction in Cases I and II and in an arbitrarily chosen direction in Case III. Study of such traces reveals that in Cases I and II the starting surfaces are macroscopically flat to within $\sim 1\,\mu$m over distances ~ 2 cm. Typically, there is a slight dome in the middle of the bar. These surfaces also are criss-crossed by two sets of ridges and valleys which run more or less perpendicular to one another. One set – the machining grooves – runs straight, parallel to the sliding direction. In Case I these grooves typically have a depth of 1 to 3 μm and a width of 10 to 30 μm, Figs. 9b and 10a; in Case II, Figs. 9d and 10b, the corresponding dimensions are 0.3 to 1 μm and 5 to 15 μm. These grooves are pock-marked with craters a few μm across, Figs. 9a and 9c, which apparently result from the pull-out of α-SiC grains, Fig. 11. The second set,

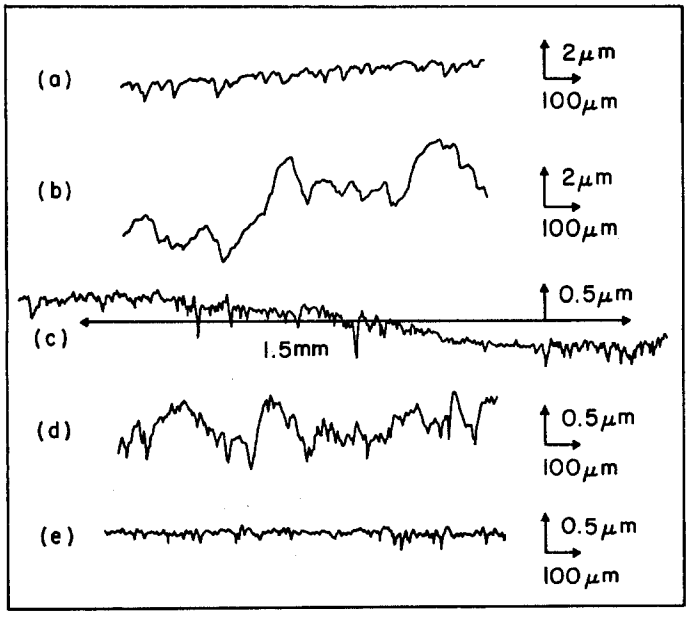

Figure 9 Profilometer traces from coarse machined ((a) and (b)), fine machined ((c) and (d)) and lapped and polished (e) specimens of α-SiC. Traces (a) and (c) run parallel to the machining direction and traces (b) and (d) perpendicular to this direction.

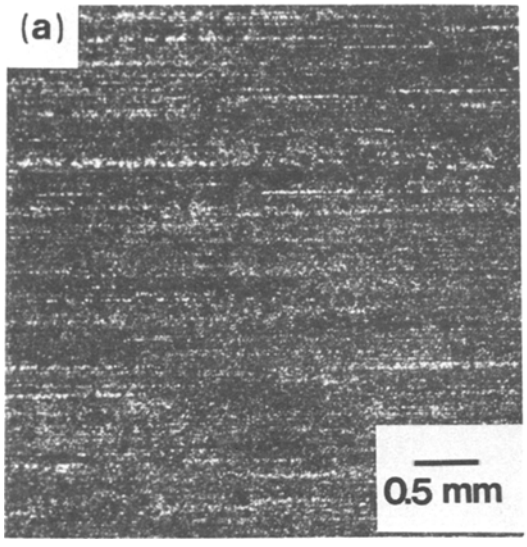

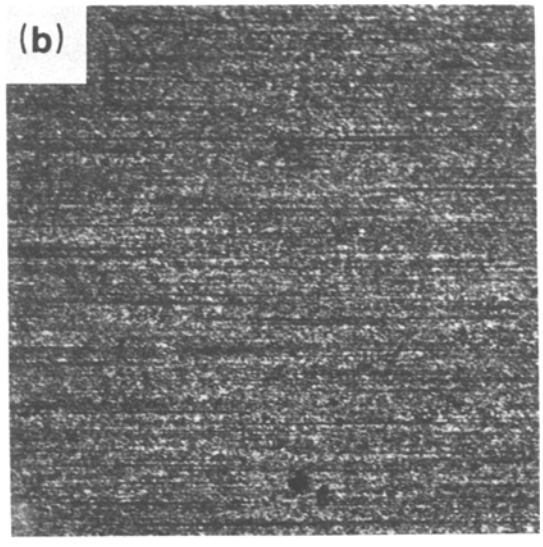

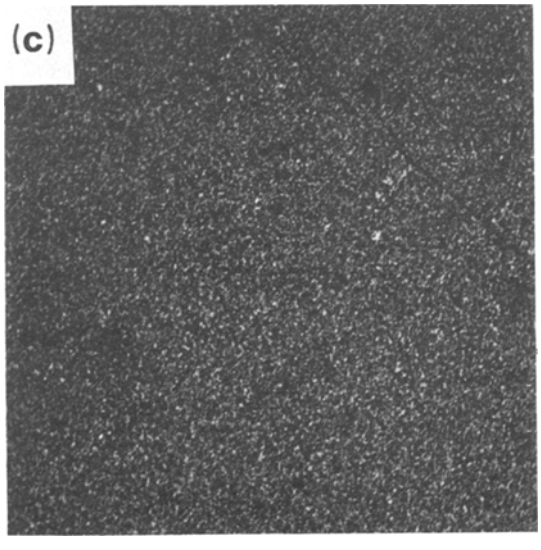

Figure 10 Optical micrographs of (a) coarse machined, (b) fine machined and (c) lapped and polished specimens of α-SiC.

which is clearly visible to the unaided eye on lightly worn samples under conditions of oblique illumination, Fig. 12, generally has an amplitude of 0.5 to 1 μm and a wavelength of 1 to 3 mm in both Case I, Fig. 9a, and Case II, Fig. 9c. These ridges and valleys are thought to be the result of vibrations set up in the specimen and the surface grinder during machining. It is noteworthy that they cannot easily be seen in either the optical or the scanning electron microscope.

In Cases III and IV of Fig. 8, the lapping and/or polishing procedures not only improve the overall flatness to $\lesssim 0.5\,\mu$m in 2 cm, but also eliminate any millimetre wavelength surface waviness and reduce the average local peak-to-valley height to $\sim 0.2\,\mu$m, Figs. 9e and 10c. There is very little difference between the lapped finish (Case IV) and that obtained by polishing after lapping (Case III).

The gradual evolution of the oscilloscope traces of F and N with increasing number of cycles of operation is reflected in changes in the

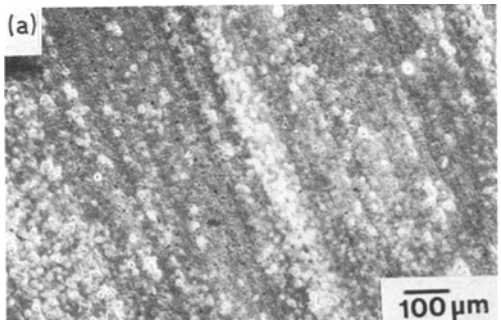

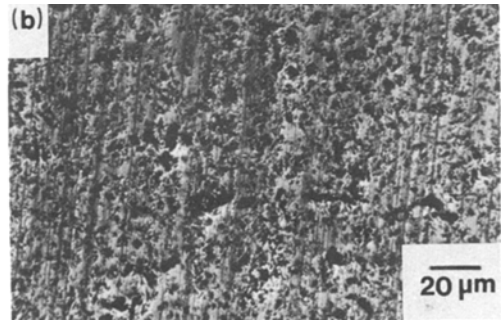

Figure 11 Craters resulting from pull-out of individual SiC grains during (a) coarse and (b) fine diamond machining of sintered α-SiC.

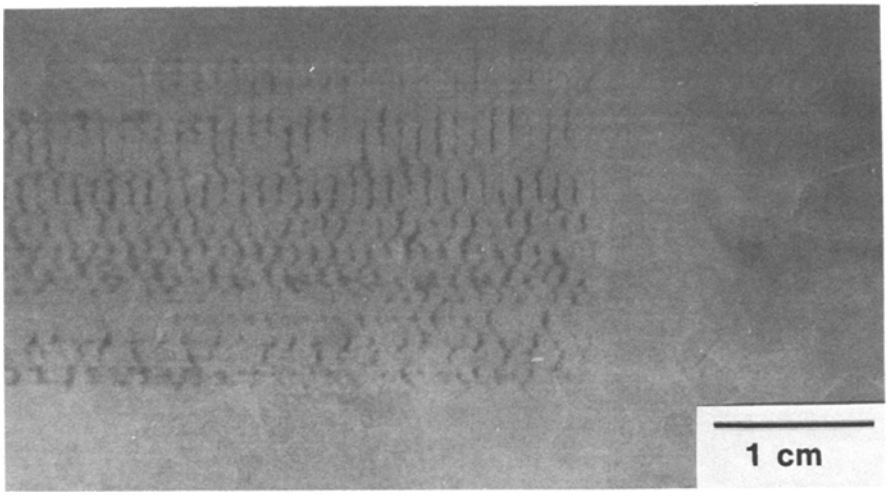

Figure 12 Ridges and valleys running perpendicular to the machining direction on α-SiC. These features are only visible under oblique illumination in regions where light wear has flattened the tops of the ridges without completely removing them.

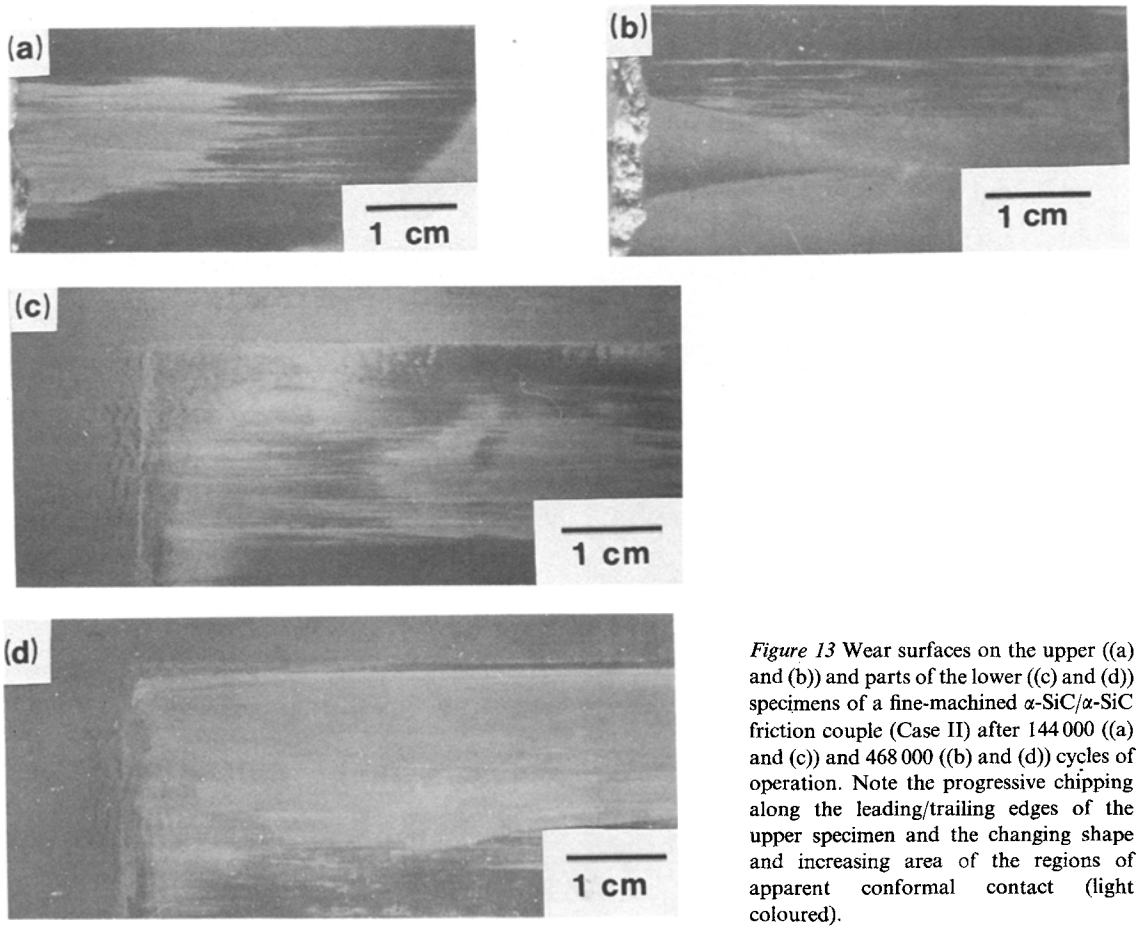

Figure 13 Wear surfaces on the upper ((a) and (b)) and parts of the lower ((c) and (d)) specimens of a fine-machined α-SiC/α-SiC friction couple (Case II) after 144 000 ((a) and (c)) and 468 000 ((b) and (d)) cycles of operation. Note the progressive chipping along the leading/trailing edges of the upper specimen and the changing shape and increasing area of the regions of apparent conformal contact (light coloured).

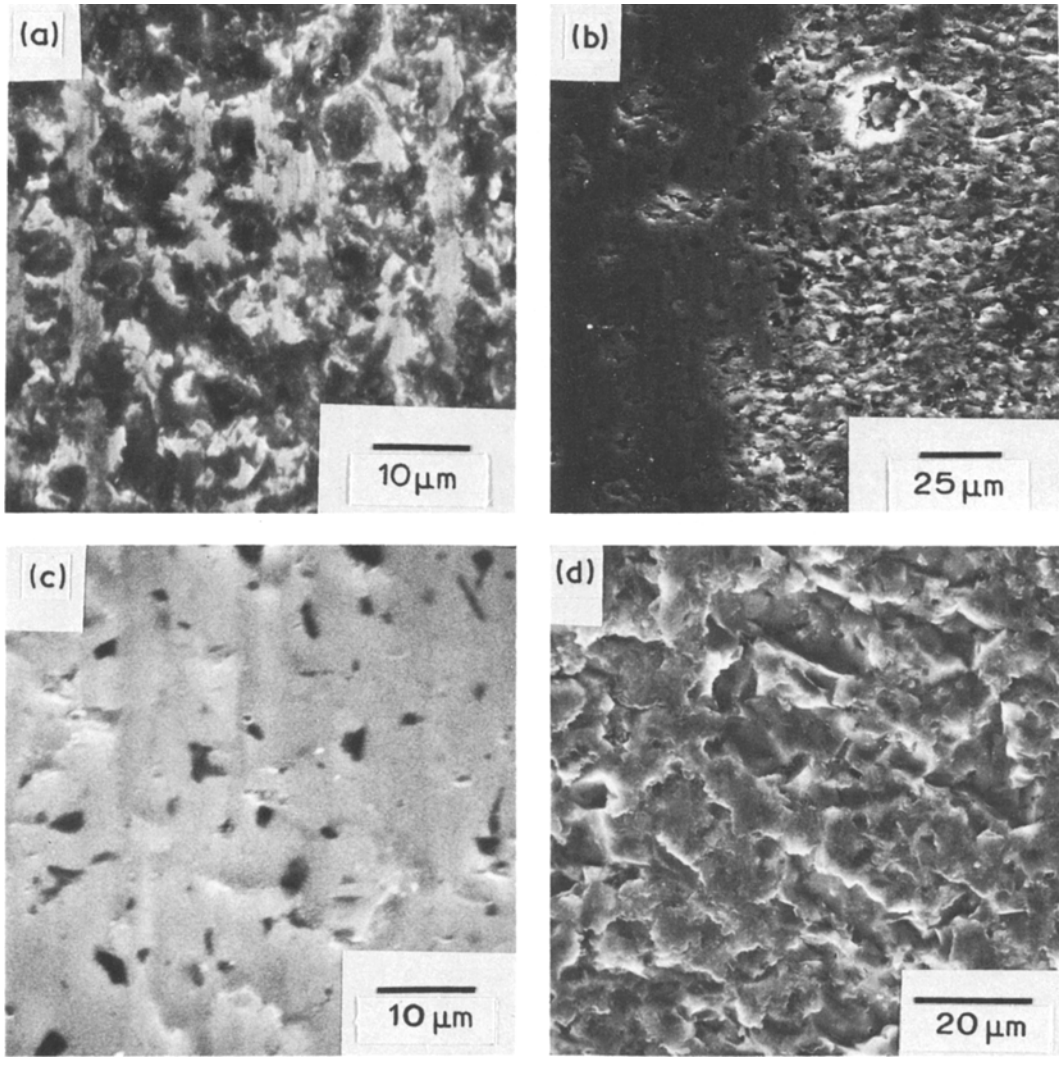

Figure 14 Coarse machined α-SiC surface (Case I) prior to the start of sliding (a) and after 864 000 cycles of operation ((b), ((c) and (d)). Wear has occurred by two quite distinct mechanisms: polishing (left-hand side of (b) and (c)) and microchipping ((right-hand side of (b) and (d)). The machining direction in (a) and the sliding direction in (b) to (d) are aligned vertically.

appearance of the sliding surfaces. Fig. 13 shows the wear surface of the upper specimen and part of the wear surface of the lower specimen in Case II after 144 000 and 468 000 cycles of operation. There is sporadic chipping away of material from the leading/trailing edges of the upper (smaller) specimen; and on both specimens the area of what appears to be conformal contact increases with increasing number of cycles. Similar behaviour was observed to varying degrees in all four cases reported in Fig. 8.

The differences in contrast observed at different points on the wear surfaces shown at low magnification in Figs. 13a to d are the results of marked differences in surface topography. Figs. 14 and 15, for example, compare wear surfaces from the friction couple employed in Case I in their initial (coarse machined) state and after 864 000 cycles of operation. Fig. 14a is a high

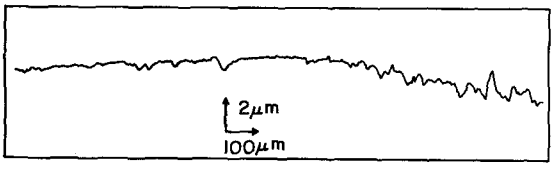

Figure 15 Profilometer trace across a boundary such as that shown in Fig. 14b. The polished region on the left is much smoother than the microchipped region on the right.

magnification scanning electron micrograph of the same surface as shown in Fig. 10a and is representative of the whole area of either specimen prior to the start of sliding. This surface exhibits evidence of grooving at some points and of grain pull-out at others, and it has the comparatively rough topography illustrated in Figs. 9a and b. Fig. 14b was taken at a location within the wear scar generated on the smaller (upper) specimen where there was a clearly visible change in surface reflectivity. It demonstrates graphically the way in which quite different wear mechanisms can co-exist across a narrow boundary. On the left side, shown enlarged in Fig. 14c, the wear surface appears to have been polished to the point that individual grains are becoming visible. In addition, there are shallow ($\sim 0.2\,\mu$m deep, Fig. 15) grooves running parallel to the sliding direction and there is little evidence either of grain pull-out or of the formation of wear debris. On the right side of the boundary the wear surface looks quite different. Again there is relatively little wear debris on the surface, even though there appears to have been extensive brittle microchipping. Fig. 14d, which was taken after the specimen was cleaned ultrasonically in acetone, shows the topography resulting from this microchipping process in greater detail. The average peak-to-valley height in this region is $\sim 1\,\mu$m, Fig. 15, which value is intermediate between the values for the starting surface ($\sim 2\,\mu$m, Fig. 9b) and the polished region ($\sim 0.5\,\mu$m, Fig. 15). It is probable that these two wear mechanisms make quite different contributions to the coefficient of friction.

The frictional behaviour of the lapped and polished (Case III) and lapped (Case IV) α-SiC specimens differs from that of the machined specimens in that the coefficient of friction tends to increase asymptotically rather than decrease asymptotically during the early stages of sliding. The anomalous "step" in Curve III of Fig. 8 between 300 000 and 400 000 cycles of operation is attributed to the trapping at the sliding interface of material chipped away from the leading/trailing edges of the smaller specimen. An example of this phenomenon on a machined specimen is shown in Figs. 13a and b. Note that this chipping process occurs on a scale much larger than the grain size. It appears that for the initially rough surfaces the coefficient of friction decreases as wear smooths out the initial machining damage and establishes the steady state wear surface topography. In contrast, the coefficient of friction of the initally smooth surfaces increases with increasing number of cycles of operation, Fig. 8, because the wear process increases the surface roughness. This surface roughening is shown clearly by the profilometer trace presented in Fig. 16. The right-hand side of this trace is a low magnification version of Fig. 9e and shows the $\sim 0.2\,\mu$m average peak-to-valley height characteristic of the starting surface; and the left-hand side shows that the average peak-to-valley height in the worn region is $\sim 1\,\mu$m. The similarity of this portion of the trace and the right-hand end of the trace shown in Fig. 15 is striking.

Fig. 17a is a scanning electron micrograph showing the surface seen in Fig. 10c at a higher magnification. It shows a lapped and polished specimen of α-SiC prior to the start of sliding. A considerable fraction of the area of this surface consists of smooth polished α-SiC grains. As seen after 468 000 cycles of operation, Fig. 17b, the worn surface is heavily obscured by micrometre and sub-micrometre size wear debris. After cleaning ultrasonically in acetone, however, it becomes apparent that the worn surface looks very much like that shown in Fig. 14d. Evidently, the mechanism of wear on a lapped and polished α-SiC surface involves the same microchipping process as does the wear on some regions of a machined surface of the same material.

Close scrutiny of Figs. 14d and 17c suggests that this microchipping process involves both intragranular and intergranular fracture. When

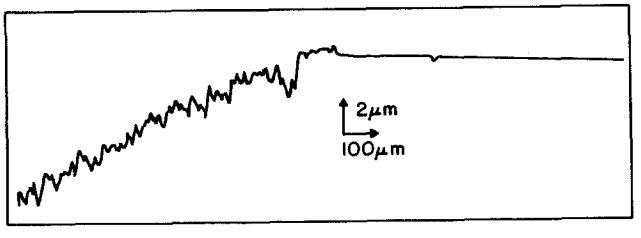

Figure 16 Wear trace across the boundary of the wear scar perpendicular to the sliding direction on an initially lapped and polished specimen of α-SiC. The right-hand end of the trace shows the unworn surface, and the left-hand end shows the much rougher topography generated by 468 000 cycles of operation.

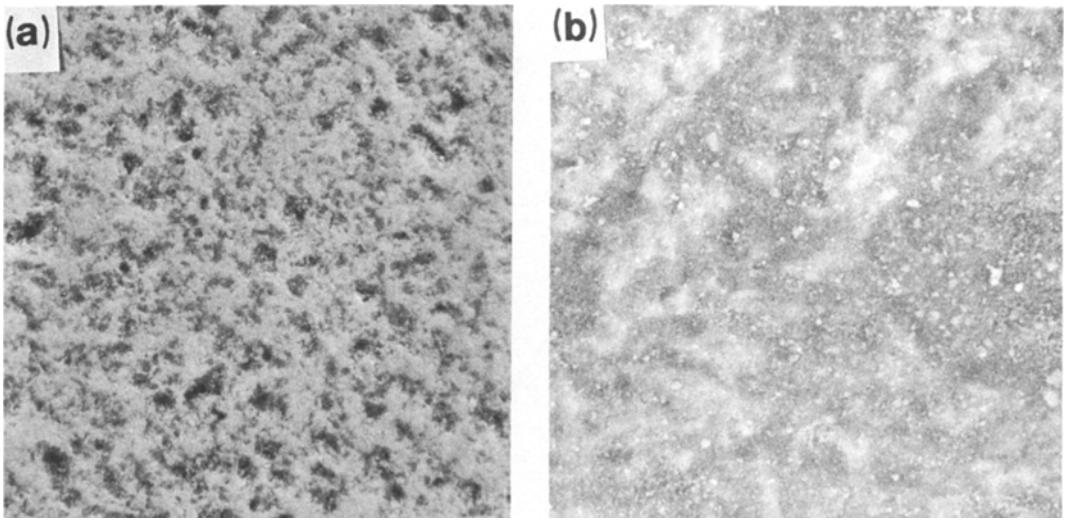

Figure 17 Lapped and polished α-SiC surface (Case III) (a) prior to start of sliding, (b) after 468 000 cycles of operation and (c) after the same amount of wear and subsequent ultrasonic cleaning. The sliding direction in (b) and (c) is horizontal.

a grain is first exposed as the surface wears down, it loses chips by brittle intragranular fracture. Then, as the surrounding material is worn away, whatever part of the grain remains at some point detaches by brittle intergranular fracture. The topography of the steady state wear surface thus has a characteristic dimension no larger than the grain size. The number of cycles of operation required to establish this steady state depends on the difference in peak-to-valley height between the initial and the steady state wear surfaces. Thus it is the coarse machined surface that takes the largest number of cycles to reach the steady state and the lapped or lapped and polished surfaces that reach this state most rapidly, Fig. 8.

This picture of the wear process in α-SiC is still far from complete. In particular it leaves unexplained (1) why polishing sometimes occurs instead of or in addition to microchipping, (2) why the coefficient of friction does not always tend to the same limit after a large number of cycles, and (3) the role of wear debris. In the present experiments there are two quite different sources of wear debris: microchipping, which produces micrometre or sub-micrometre particles between the sliding surfaces; and the larger scale chipping along the leading/trailing edges of the smaller specimen, which produces much larger particles that presumably can become entrapped at the sliding interface. The former process is an integral part of the friction behaviour, but the latter is an unwanted extraneous factor. Another possible extraneous complication is that the coefficient of friction μ_f is calculated as $|\bar{F}|/\bar{N}$ rather than as $(\overline{|F|/N})$. It is suggested that these two extraneous factors may account for the observed variation of the steady state value of μ_f between 0.30 and 0.45.

4.2. Sliding behaviour of like pairs of materials

Fig. 18 shows the temporal dependence of the coefficient of friction for like pairs of fine-machined α-SiC, C–SiC, Si–SiC and PSZ. Since the experimental conditions were the same as in

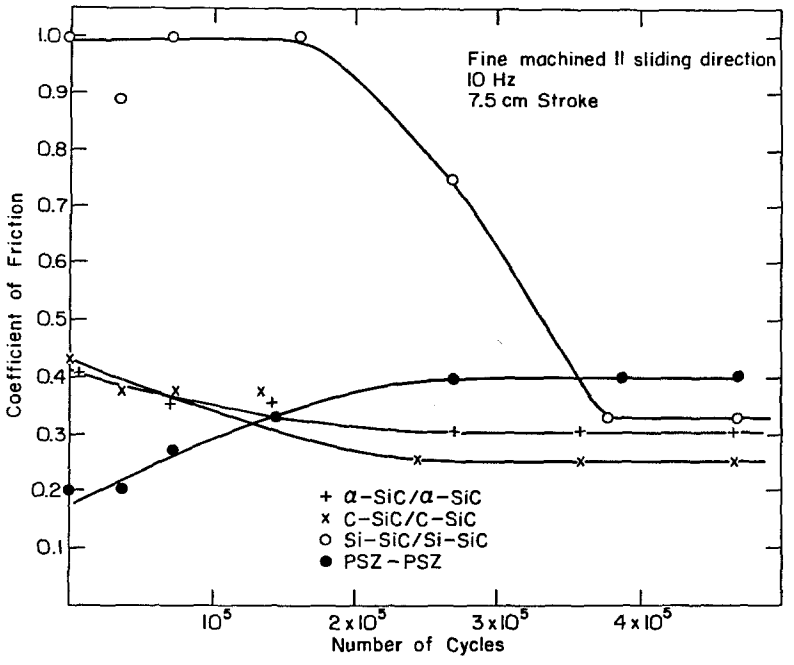

Figure 18 Variation of the coefficient of friction with number of cycles of sliding wear for like pairs of materials.

the preceding section, the α-SiC/α-SiC curve in Fig. 18 is merely a reproduction of Curve II of Fig. 8. It is noteworthy that all four materials exhibit quite similar values of the coefficient of friction (0.33 ± 0.07) once steady state wear is achieved, even though their initial values of this parameter are widely different.

In the case of C–SiC, the coefficient of friction decreased asymptotically from 0.40 to 0.25, which latter is the lowest steady state value observed in the present work. Comparison of micrographs of the initial and steady state wear surfaces, Fig. 19, and of the corresponding profilometer traces parallel and perpendicular to the sliding direction, Fig. 20, shows that the decrease in the coefficient again results from polishing, i.e., surface smoothing. Fig. 20 shows that there is much more smoothing perpendicular to the sliding (and machining) direction than parallel to it. It is clear that the machining grooves present at the start of the experiment are eliminated by the wear process, but the mechan-

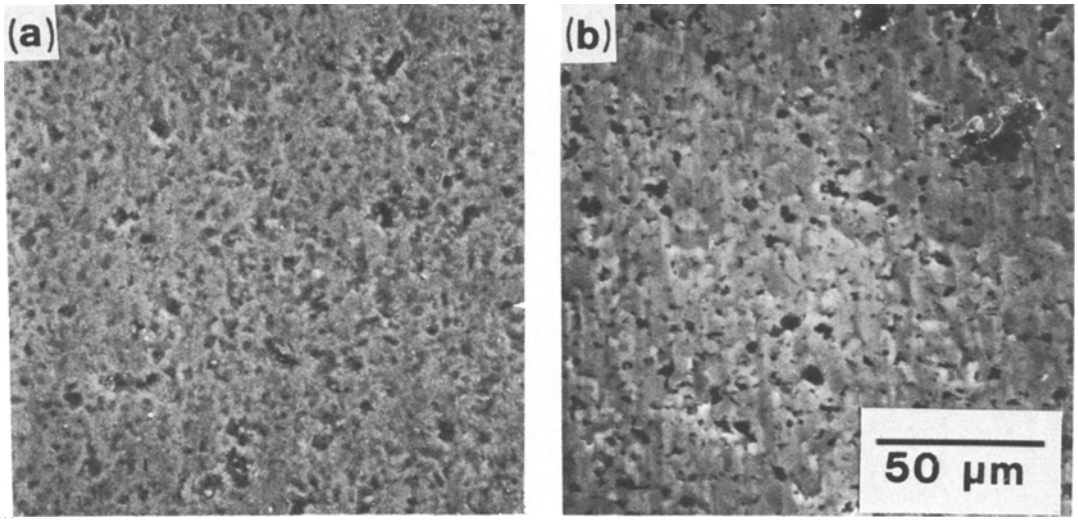

Figure 19 The surface of fine machined C–SiC (a) before and (b) after 468 000 cycles of sliding wear. The machining direction in (a) and the sliding direction in (b) run vertically.

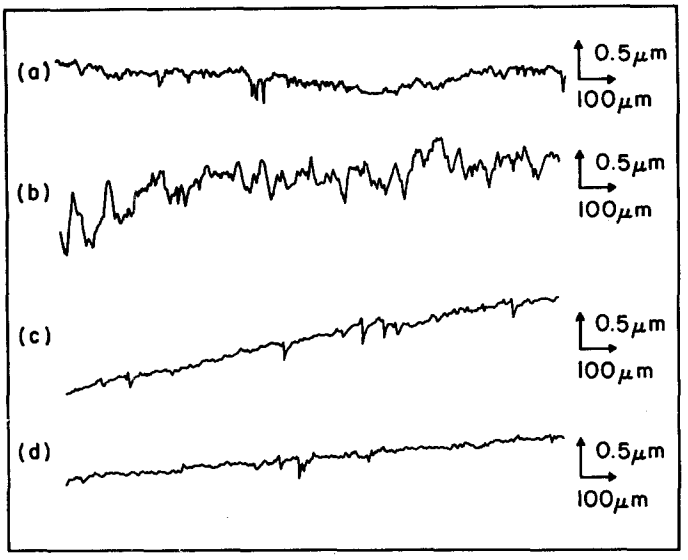

Figure 20 Profilometer traces parallel ((a) and (c)) and perpendicular ((b) and (d)) to the sliding direction on unworn ((a) and (b)) and worn ((c) and (d)) C–SiC.

ism by which this happens is not obvious. At the level of resolution obtainable in the scanning electron microscope used in the present work it is not possible to identify the possible contributions of very fine scale chipping of the SiC, plastic deformation of the SiC, and smearing (by plastic deformation) of the graphite present in the material. Its somewhat lower steady state coefficient of friction as compared to α-SiC or Si–SiC suggests that this last process does occur in C–SiC, enabling the graphite to act as a solid lubricant.

The behaviour of the Si–SiC/Si–SiC friction couple provides a marked contrast to that of the C–SiC/C–SiC couple. Fig. 18 shows that the initial value of the coefficient of friction is very high ($\gtrsim 0.9$) and that there is a precipitous drop to the steady state value of 0.33 between 200 000 and 300 000 cycles of sliding wear. The Si–SiC/Si–SiC couple also differs from the α-SiC/α-SiC couples and the C–SiC/C–SiC couple in that this decrease in friction coefficient is accompanied by overall surface roughening rather than surface smoothing. Fig. 21a shows the initial machined surface, which has average peak-to-valley heights of ~ 0.2 and $\sim 1\,\mu$m along and across the machining grooves, respectively, Figs. 22a and b. After 468 000 cycles of sliding, however, these heights have both increased to 3 to 4 μm, Figs. 22c and d. The worn surface, Figs. 21b and c, has a complex topography made up of small, isolated smooth areas surrounded by larger rough areas. These smooth areas exhibit shallow grooves running parallel to the sliding direction. It was not possible in this work to relate any of these topographical features to the distribution of Si and SiC in the microstructure.

The final like friction couple studied, PSZ/PSZ, exhibited at least an order of magnitude more wear than any of the SiC/SiC couples studied. In the course of 468 000 cycles of sliding – equivalent to no more than a few hours of idling for an automobile engine – the smaller (upper) specimen wore down in thickness from 1 to ~ 0.5 cm. Concomitantly, the coefficient of friction rose from an initial value of 0.2 to a steady state value of 0.4. This latter value is higher than the corresponding value for any other of the like pairs studied in the fine machined starting condition. Figs. 23a and 24b show that the initial surface consists of smooth machining grooves 0.3 to 0.4 μm deep. Along the grooves the average peak-to-valley height is < 100 nm, Fig. 24a. Study of the worn surface was complicated by two factors – roughening on a scale too coarse to be studied by scanning electron microscopy and surface profilometry, Fig. 23b, and adherence of widely differing amounts of wear debris at different locations, Fig. 23c. Figs. 23e and f are enlargements of the areas designated by arrows in Fig. 23c. The former micrograph shows a region completely covered by a dense layer of micrometre size wear particles; and the latter shows an area which, despite its smoother appearance, is obscured at its centre by adherent wear debris. In regions substantially free of wear

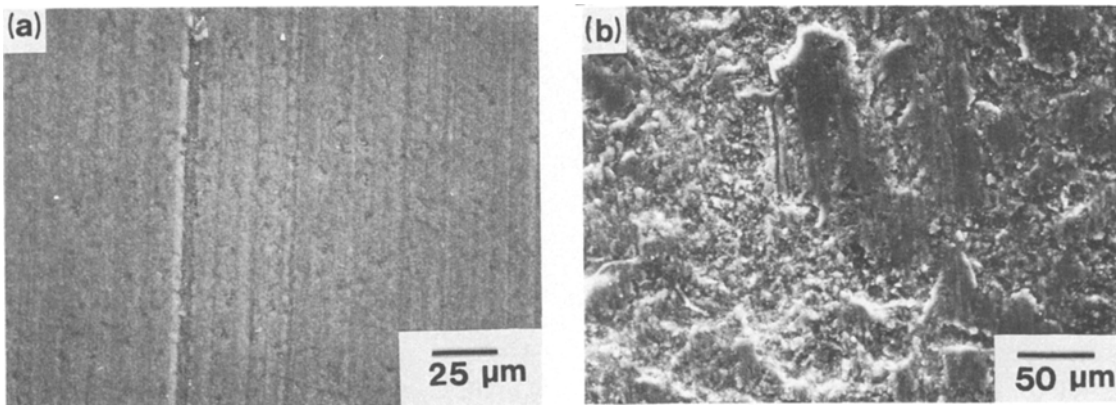

Figure 21 The surface of fine machined Si–SiC (a) before and ((b) and (c)) after 468 000 cycles of sliding wear. The machining direction in (a) and the sliding direction in (b) and (c) runs vertically.

debris, whether naturally, as on the right-hand side of Fig. 23f, or as the result of cleansing ultrasonically, as in Figs. 23b and d, the wear surface is seen to be deeply grooved parallel to the sliding direction. The plateau B seen in Fig. 23b stands $\sim 150\,\mu$m above the plains A and C, which themselves differ in elevation by $\sim 25\,\mu$m. By comparison with such gross features, plains such as A and C are relatively flat, although they are still much rougher than the initial surface. Fig. 24d shows that the grooves seen in such plains after ultrasonic cleaning, Fig. 23d, are 2 to $3\,\mu$m deep; and Fig. 24c reveals that the peak-to-valley height along these grooves is 1 to $2\,\mu$m. The significance of this latter figure is difficult to determine because the grooves are not everywhere continuous or parallel. As in the case of the SiC materials, the scanning electron microscope did not provide the resolution necessary to elucidate the separate roles of flow and fracture processes in groove and wear debris formation.

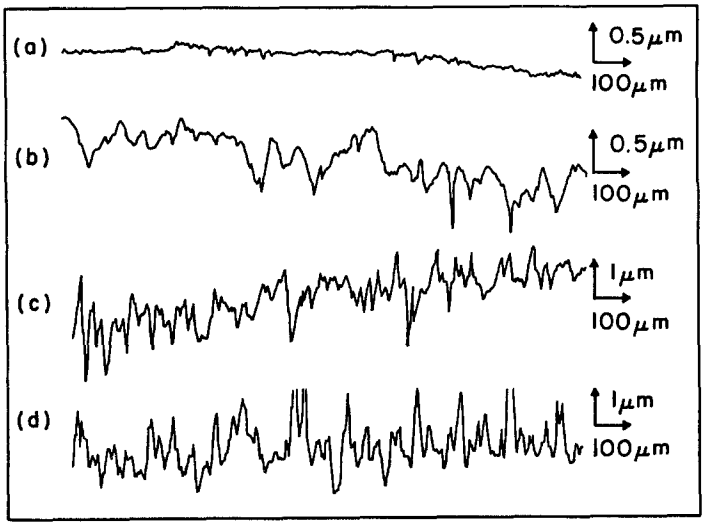

Figure 22 Profilometer traces parallel ((a) and (c)) and perpendicular ((b) and (d)) to the sliding direction on unworn ((a) and (b)) and worn ((c) and (d)) Si–SiC.

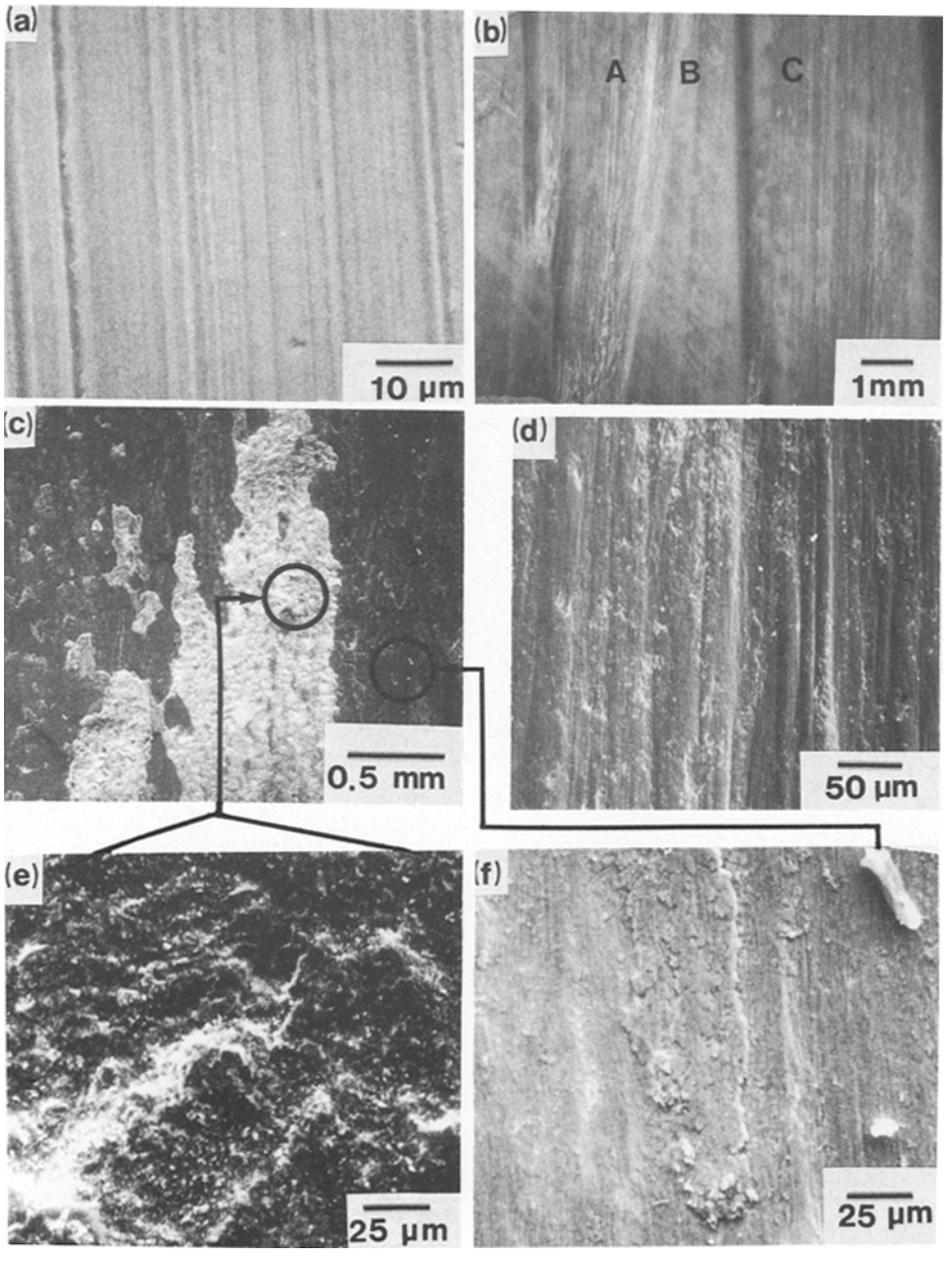

Figure 23 The surface of fine-machined PSZ (a) before and ((b) to (f)) after 468 000 cycles of sliding wear. (b) is a low magnification optical micrograph taken under oblique illumination. The plateau B stands $\sim 150\,\mu$m above the areas A and C, which themselves differ in elevation by $\sim 25\,\mu$m. (e) and (f) are enlargements of the indicated areas of (c) showing thick and thin layers of adherent wear debris, respectively. (d) shows a small part of an area of the wear surface such as A or C in (b) after ultrasonic cleaning. In each micrograph the machining and/or sliding direction is set vertical.

It also provided no information about the possible role of stress-induced phase transformations at the contact interface in determining the tribological behaviour.

4.3. Sliding behaviour of unlike pairs of materials

Three friction couples consisting of fine machined unlike pairs of materials were also tested.

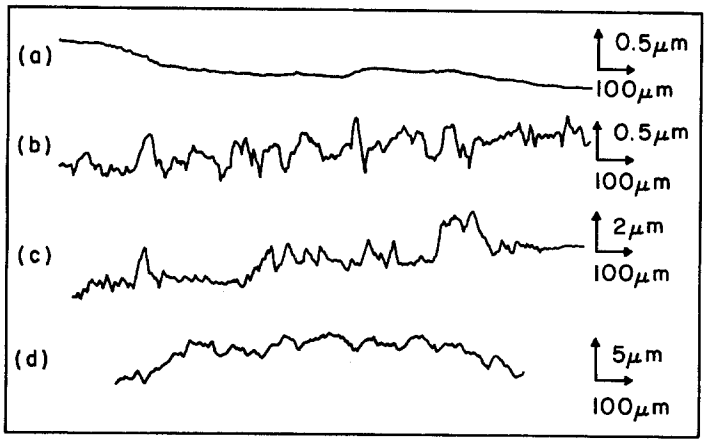

Figure 24 Profilometer traces parallel ((a) and (c)) and perpendicular ((b) and (d)) to the sliding direction on unworn ((a) and (b)) and worn ((c) and (d)) PSZ. (c) and (d) come from an area such as A or C in Fig. 23b.

Small specimens of PSZ, Si–SiC and C–SiC were slid on large specimens of α-SiC, C–SiC and PSZ, respectively. Except that the α-SiC specimen was machined perpendicular rather than parallel to the sliding direction, the experimental conditions were the same as for the like pairs. Fig. 25 shows the friction data obtained. The steady state coefficients of friction vary between 0.4 and 0.5. In the two cases where one member of the friction couple is PSZ, the coefficient of friction is initially low and increases asymptotically to its steady state value over ~ 50 000 cycles of operation. In the third case, Si–SiC/C–SiC, the coefficient of friction is initially high (~ 0.63) and decreases asymptotically to its steady state value of 0.43 after ~ 100 000 cycles of operation.

Fig. 26 shows the wear surfaces of the PSZ/α-SiC couple after 270 000 cycles of sliding wear followed by ultrasonic cleaning. The corresponding profilometer traces are presented in Fig. 27. The wear surface on the PSZ half of the couple varies greatly in topography from location to location – so much so that it is not possible to characterize the roughness either parallel or perpendicular to the sliding direction by means of a single profilometer trace. Figs. 27a and b are thus composites made up of sections of several parallel traces. They show that the peak-to-valley height can vary between ~ 0.2 and ~ 3 μm along a trace parallel to the sliding direction. The corresponding figure for the like PSZ/PSZ couple is 1 to 2 μm, Fig. 24c. Perpendicular to the sliding direction, the PSZ member of the unlike couple developed a surface with a

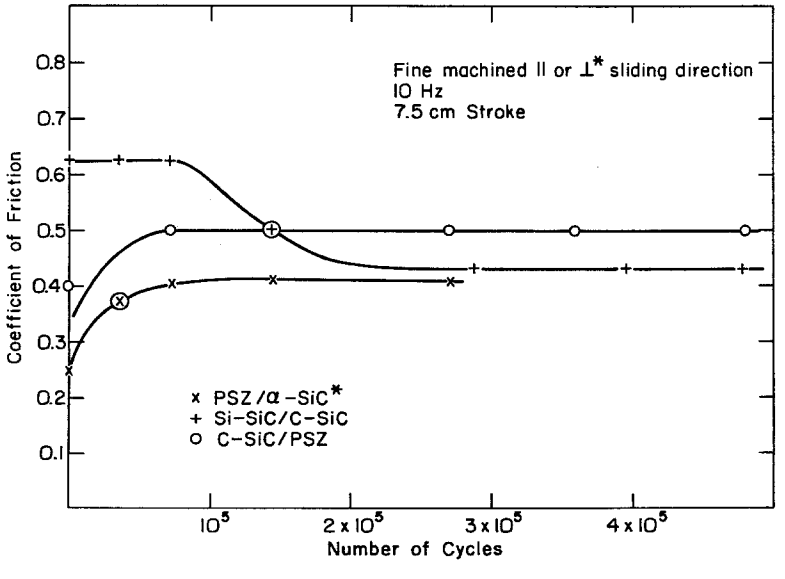

Figure 25 Variation of the coefficient of friction with number of cycles of sliding wear for unlike pairs of materials.

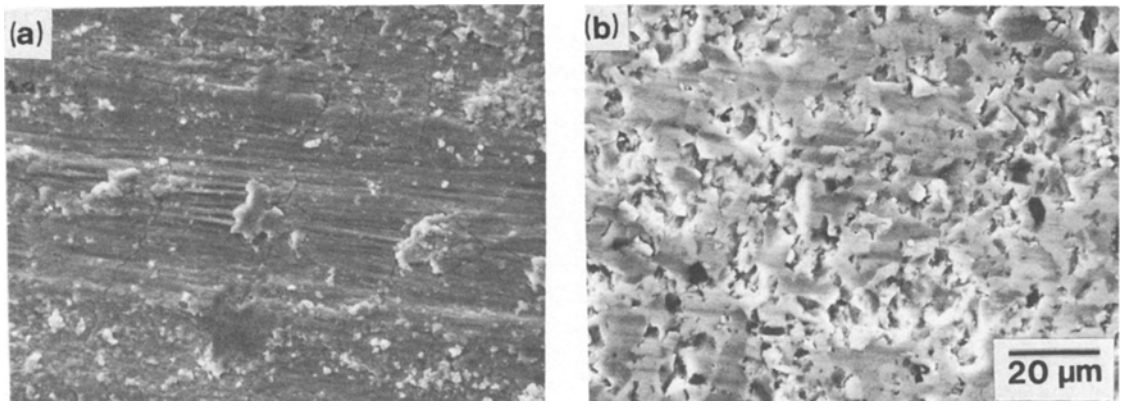

Figure 26 Surfaces of PSZ (a) and α-SiC (b) worn by 270 000 cycles of sliding against one another. The sliding direction runs horizontally.

peak-to-valley height varying at different locations from ~0.2 to ~8 μm, Fig. 27b. Such variations in topography are nothing like as extreme as those observed on the worn surfaces of the like PSZ/PSZ couple, Figs. 23b and d, but they suggest the onset of a similar wear process.

Close examination of Fig. 26a shows that even after ultrasonic cleaning the wear grooves in some places remain obscured by adherent wear debris particles, at least some of which appear to be larger than the grain size (cf. Fig. 6). Also visible in Fig. 26a is a more-or-less rectangular network of fine cracks, the longer segments of which run perpendicular to the grooves and the shorter segments of which run parallel to the grooves. At the present time it is neither clear when in the wear process these cracks form nor what might be their role in the formation of the wear debris. It is possible that they are caused by thermal shock.

Comparison of Fig. 26b with Figs. 14c and d suggests that the α-SiC member of the PSZ/α-SiC couple polished at some locations even as it microchipped at other, immediately adjacent

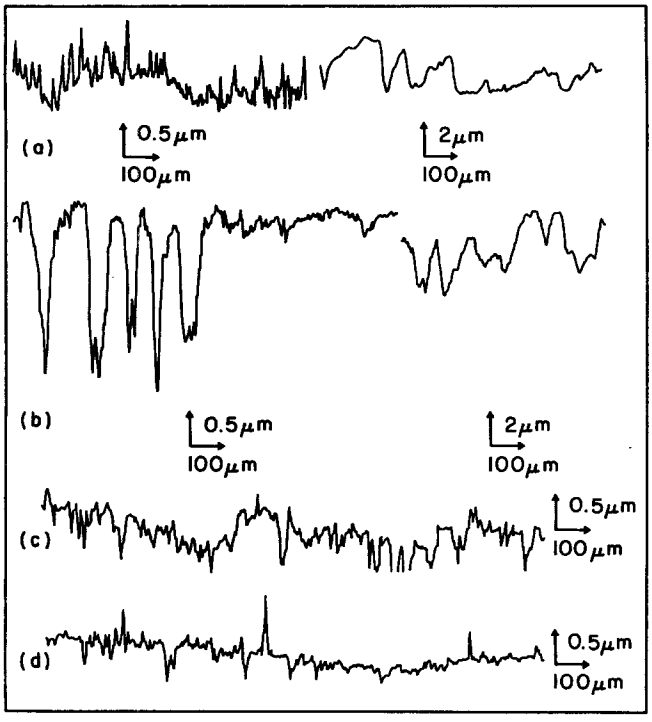

Figure 27 Profilometer traces parallel ((a) and (c)) and perpendicular ((b) and (d)) to the sliding direction on worn PSZ ((a) and (b)) and worn α-SiC ((c) and (d)).

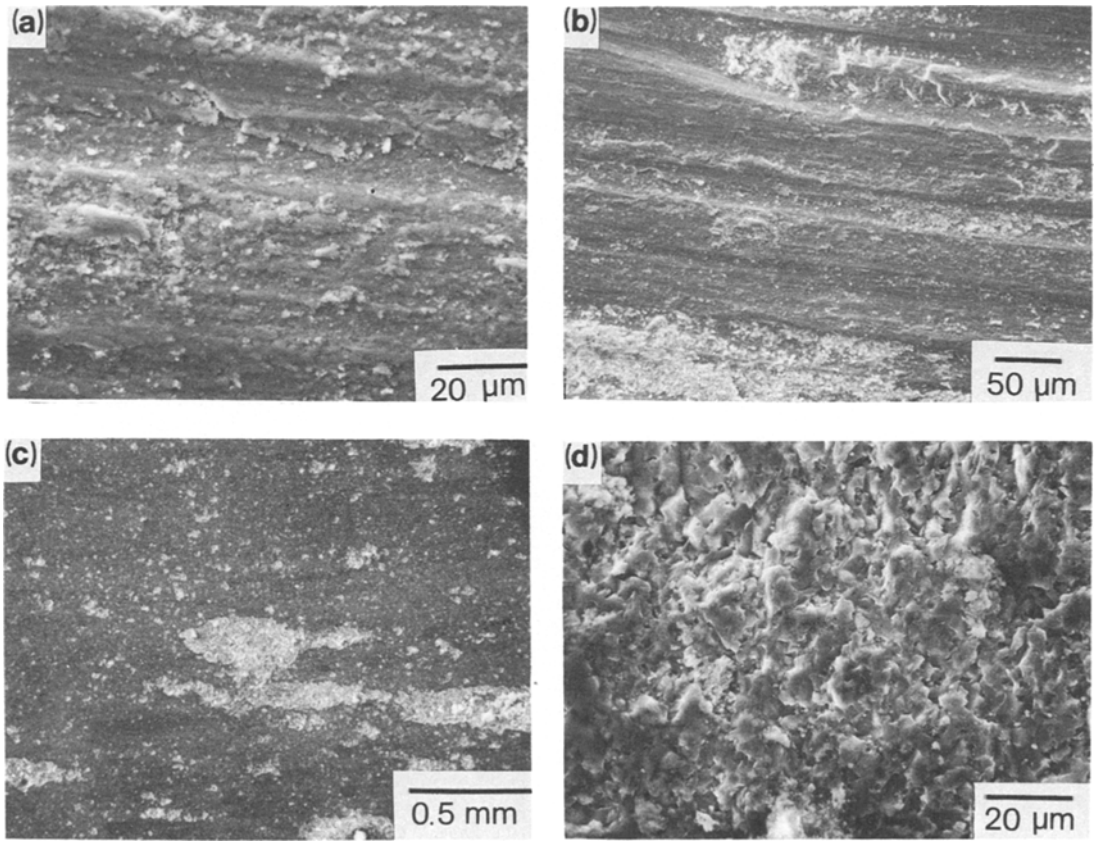

Figure 28 The worn surfaces of a PSZ ((a) and (b))/C–SiC ((c) and (d)) friction couple after 468 000 cycles of sliding wear and ultrasonic cleaning. The sliding direction runs horizontally.

locations. This specimen was machined perpendicular rather than parallel to the sliding direction. Hence the profilometer trace of the worn surface parallel to the sliding direction Fig. 27c, should be compared with Fig. 9d; and that perpendicular to the sliding direction, Fig. 27d, should be compared to Fig. 9c. When the comparisons are made, it is seen that the overall effect of 270 000 cycles of sliding wear is to roughen the surface perpendicular to the sliding direction (i.e., parallel to the original machining grooves) without producing any significant change in roughness parallel to the sliding direction. The peak-to-valley heights on the worn surface are 0.3 to 0.7 μm and 0.2 to 0.5 μm parallel and perpendicular to the sliding direction, respectively.

In the case of C–SiC sliding on PSZ, there is again substantial and oft-times variable roughening of the PSZ accompanied by the formation of an adherent layer of wear debris, some parts of which persist even after ultrasonic cleaning. Figs. 28a and b show, respectively, partly debris-covered and largely debris-free regions of the wear surface resulting from 468 000 cycles of sliding wear after it had been ultrasonically cleaned. The similarity between Figs. 28a and 26a on the one hand and between Figs. 28b and 23d on the other emphasizes that PSZ wears by a common mechanism when sliding against itself, α-SiC and C–SiC. Fig. 28a even exhibits a less well-defined version of the network of fine cracks seen in Fig. 26a; and Figs. 29a and b demonstrate that the range of peak-to-valley heights parallel and perpendicular to the wear grooves produced on PSZ by sliding it against C–SiC (0.6 to 1.0 μm and 1 to 5 μm, respectively) fall within the range of those produced by sliding it against α-SiC. Further evidence of this commonality of wear mechanism is provided by Figs. 18 and 25, which show that friction couples including PSZ exhibit a higher steady state than initial coefficient of friction.

In contrast, the wear of the α-SiC and C–SiC

Figure 29 Profilometer traces parallel ((a) and (c)) and perpendicular ((b) and (d)) to the sliding direction on PSZ ((a) and (b)) and C–SiC ((c) and (d)) surfaces subjected to 468 000 cycles of sliding wear against one another.

counterfaces exhibits significant differences. Whereas the regions within which either microchipping or polishing dominated were small and intimately juxtaposed in the case of α-SiC, Fig. 26b, the C–SiC wear surface developed quite large, contiguous regions of microchipping damage, Figs. 28c and d. These regions manifest themselves as occasional 1 to 2 μm deep "spikes" on the profilometer traces obtained from the worn surface parallel, Fig. 29c, and perpendicular, Fig. 29d, to the sliding direction. Between these chipped regions, the polished surface has an average peak-to-valley height of only 100 to 200 nm. It is not clear whether this difference in wear surface topography arose because the C–SiC was subjected to nearly twice as many cycles of wear as the α-SiC, because the α-SiC was machined perpendicular to the sliding direction rather than perpendicular to it as was the C–SiC, or because of the difference in microstructure between the two materials (the C–SiC contains more pores and more graphite, Table I and Figs. 4 and 5). If the microchipping process is indeed autocatalytic, in the sense that once it begins (at a pore or at the site of particularly intensive machining damage?) it provides along the edges of the resultant wear scar preferred sites for its further occurrence [17], it might well develop more extensively in C–SiC than in α-SiC, despite the greater availability in the former of graphite to act as a solid lubricant.

Figs. 30 and 31 present scanning electron micrographs and profilometer traces obtained from ultrasonically cleaned specimens of Si–SiC and C–SiC which had previously been subjected to 468 000 cycles of sliding wear against one

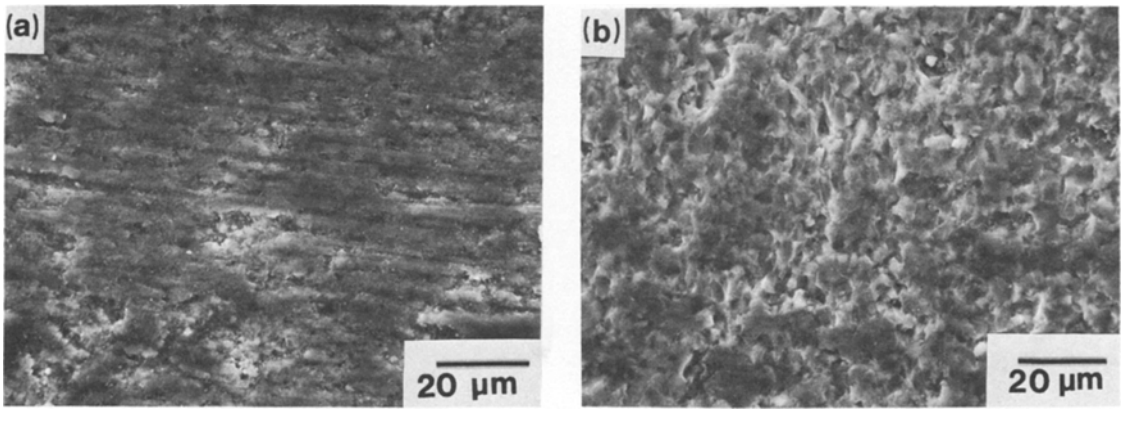

Figure 30 The worn surfaces of Si–SiC (a) and C–SiC (b) specimens subjected to 468 000 cycles of sliding wear against one another. Both surfaces have been cleaned ultrasonically. The sliding direction runs horizontally.

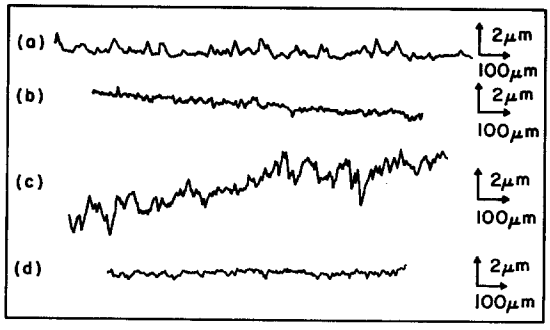

Figure 31 Profilometer traces obtained parallel ((a) and (c)) and perpendicular ((b) and (d)) to the sliding direction from the members of an Si–SiC ((a) and (b))/C–SiC ((c) and (d)) friction couple subjected to 468 000 cycles of wear.

another. Both specimens have extensively polished surfaces, and both exhibit comparatively little evidence of microchipping, Figs. 30a and b. Nevertheless, the steady state coefficient of friction is not significantly lower than for couples which wear far more heavily. A curious feature of the topographies of both wear surfaces is that they are rougher parallel to the sliding (initial fine machining) direction than perpendicular to it. Examination of Figs. 31a and b reveals average peak-to-valley heights of 0.5 to 1 μm along and 0.3 to 0.5 μm across the wear grooves on the Si–SiC member of the couple; and Figs. 31c and d yield corresponding figures of 0.5 to 2 μm and 0.3 to 0.5 μm for the C–SiC member.

5. Concluding remarks

It is of interest to compare the results of the present work where possible with those of past studies of the sliding behaviour of similar combinations of materials in similar contact geometries.

To begin with, it is noted that all of the steady state coefficients of friction recorded in the present work fall within or only slightly without the range of values (0.3 to 0.4) suggested by Rabinowicz [18] as being "typical of unlubricated non-metals sliding on themselves".

For the SiC materials specifically, various of the present findings may be compared with the results obtained recently by Miyoshi and Buckley [19], Adewoye and Page [20] and Richerson *et al.* [21, 22]. Miyoshi and Buckley reported a coefficient of friction of 0.55 at room temperature for a single pass of one argon sputter-cleaned flat SiC single crystal over another in a vacuum of 10^{-8} Pa. This coefficient rose to 0.70 when the SiC surfaces were reacted with air prior to testing, which value is comparable with the initial value obtained from the coarse machined α-SiC/α-SiC couple.

A rather wider range of values was reported by Adewoye and Page [20], who slid 60° and 90° conical styli made of hot-pressed SiC (Norton NC203) over flat samples of the same material and of a reaction sintered SiC (Refel). The flat surfaces had 0.25 μm finishes, i.e., they were somewhat smoother than the fine machined surfaces employed in the present work and comparable in roughness with the present lapped and lapped and polished samples of α-SiC. Adewoye and Page performed their experiments in air at room temperature, using an unspecified speed of sliding. For a single pass of NC203 over either Refel or NC203, the coefficient of friction varied in much the same manner as the normal load was increased. At loads less than the critical load required to produce conchoidal fracture of the substrate about the region of contact, this coefficient was ~ 0.1; and at loads greater than this critical load it was ~ 0.4. The former value is significantly lower than any friction coefficient measured in the present work, which tends to support the contention that experiments with sharp styli are inappropriate guides to the tribological behaviour of ceramics in engine applications. The higher value is comparable with the steady state values obtained from all the variously finished α-SiC/α-SiC couples, from the like fine machined C–SiC/C–SiC and Si–SiC/Si–SiC couples, and from the unlike fine-machined Si–SiC/C–SiC couple.

Under reciprocating (multi-pass) conditions at a load less than the critical value, Adewoye and Page found that the coefficient of friction for the like NC203/NC203 pair rose from an initial value of 0.7 to a peak value of 1.4 and then started to decrease. The experiment was terminated after 400 passes, with the friction coefficient down to ~ 0.4 and apparently still decreasing. They do not explain why this experiment yielded an initial value of the coefficient of friction several times that observed in their single pass experiment. Although it is not possible to rationalize their multi-pass data with the results of the present work, it is interesting to note that Adewoye and Page observed on their worn surfaces the same diversity of wear

processes as seen by the present authors. They report evidence of extensive intergranular fracture, of polishing, and of plastic deformation. Evidence of the simultaneous occurrence of "grooving by plastic deformation" and microfracturing has also been reported by Moore and King [23] for the abrasion of a reaction-bonded SiC (containing 8 to 12% free Si) on SiC paper. These authors further reported seeing relatively more grooving and less fracturing on finer abrasive papers.

The range of values of the coefficient of friction reported by Richerson *et al.* [21, 22] is rather narrower. These authors studied the behaviour of α-SiC/α-SiC couples in air at room temperature at the very slow sliding speed of 8×10^{-6} m sec^{-1}. They peformed single pass tests in both "point" and "line" contact configurations. In the first case the contact radii were 3.2 mm and the loads ranged from ~ 50 to 250 N, giving rise to nominal contact areas a few hundreds of micrometres across; and in the second case they employed contact radii of 3.2 mm and infinity perpendicular and parallel to the line of contact, respectively, and loads of 5 to 45 N. The coefficient of friction appeared to be independent of the load and varied between 0.2 and 0.4 in the first case and between 0.30 and 0.36 in the second. These latter values in particular are in good agreement with the data presented in Fig. 8.

The only friction data that could be found in the literature for the unlubricated sliding of ZrO_2 on ZrO_2 is a value of 0.60 quoted by Peterson and Murray [24]. This comes from work by Rabinowicz and Imai [25], who used a pin-on-disc configuration to study the friction behaviour of a ZrO_2 of unspecified composition and microstructure in N_2 at a sliding speed of 0.046 m sec^{-1}. Rabinowicz and Imai's value is ~ 50% higher than the steady state coefficient of friction recorded for the couple PSZ/PSZ in the present work.

In the case of metal/metal friction couples, the coefficient of friction typically is (1) lowest and (2) more-or-less independent of surface roughness over the range of finish of most interest for engineering applications [18]. It increases for rougher surfaces because of interlocking of asperities and for smoother surfaces because these permit greater adhesion and a concomitant increase in the real area of contact. In the case of ceramics, however, it seems reasonable to suppose that adhesion will be more difficult and that the increase in the coefficient of friction as the opposing surfaces get smoother will therefore be less marked. The reason is that the condition for formation of an adhesive bond is more stringent in the case of a ceramic, particularly when there is a significant covalent contribution to the cohesive bonding. Metals form non-directional bonds, and so for adhesion to occur it is merely necessary to bring the atoms involved into sufficiently close proximity. For ceramics, in contrast, there is an additional orientation requirement. This may be the reason why the coefficients of friction for like couples of such brittle materials as Westerly granite, quartz, microcline, hornblende and calcite all decrease continuously with decreasing surface roughness [26].

It is therefore interesting to note that much of the present data exhibited the same trend: the initial values of the coefficient of friction of the like α-SiC/α-SiC couples increased with increasing surface roughness, Fig. 8; and for these couples, for the like couples C–SiC/C–SiC and PSZ/PSZ, and for the unlike couples PSZ/α-SiC and C–SiC/PSZ, increases in surface roughness at any stage of their lives were always accompanied by an increase in the coefficient of friction. The only exceptions to this pattern of behaviour were Si–SiC/Si–SiC and Si–SiC/C–SiC, the first of which exhibited a very large drop in friction coefficient as it roughened both parallel and perpendicular to the sliding direction, and the second of which showed a much smaller drop as it roughened parallel to the sliding direction and smoothed out perpendicular to this direction. This different behaviour of Si–SiC must have its origins in the fact that this is a two-phase material in which the SiC grains are (1) finer and (2) embedded in a matrix which is at once less hard, less stiff and less tough: but full explanation will require a far more detailed study than the present of the way in which the topographies of differently prepared surfaces evolve as the coefficient of friction approaches its steady state value.

The important practical conclusion to emerge from this work is that none of the materials studied – even the C–SiC – is likely to be very useful in a working engine without proper lubrication. The steady state coefficient of friction is

in all cases too high ($0.25 \leqslant \mu_f \leqslant 0.50$) to permit the friction losses to be reduced to acceptable levels. Further, though no quantitative measurements of wear rate were made in this work, it is clear both from the amount of wear debris collected and from the various micrographs and profilometer traces presented herein that the wear rates observed even in the present relatively mild wear environment are practically unacceptable. Analysis of the wear debris collected is presently underway. The results will be presented in a follow-on paper.

Acknowledgements

Work supported by Sohio Engineered Materials Co.

References

1. A. L. ROBINSON, *Science* **187** (1975) 1185.
2. *Idem, ibid.* **188** (1975) 40.
3. R. N. KATZ, *ibid.* **208** (1980) 841.
4. A. F. McLEAN, *Amer. Ceram. Soc. Bull.* **61** (1982) 861.
5. D. F. GODFREY, "The Use of Ceramics for Engines", p. 27 in Science of Ceramics 12, edited by P. Vincenzini, (Ceramurgica s.r.l., Faenza, Italy, 1984).
6. F. P. BOWDEN and D. TABOR, "The Friction and Lubrication of Solids", Vol. I (1954) and Vol. II (1964) (Oxford University Press, Oxford, England).
7. D. TABOR, *J. Lubrication Technol.* **130** (1981) 169.
8. D. TABOR, "Future Directions of Research in Adhesion and Friction", in "Tribology in the '80s", Vol. 1 (NASA CP-2300, NASA, Washington, DC, 1984) p. 119.
9. "Surface Effects in Crystal Plasticity" edited by R. M. Latanision and J. T. Fourie, (Noordhoff, Leyden, Holland, 1977).
10. "Atomistics of Fracture", edited by R. M. Latanision and J. R. Pickens (Plenum, New York, 1983).
11. J. F. O'HANLON, "A User's Guide to Vacuum Technology", (Wiley, New York, 1980) pp. 8 *et seq.*
12. S. ROBB, *Amer. Ceram. Soc. Bull.* **62** (1983) 755.
13. L. B. SIBLEY, private communication (1984).
14. A. F. WELLS,"Structural Inorganic Chemistry", 3rd Edn., (Oxford University Press, Oxford, England, 1962) p. 768.
15. H. G. SCOTT, *J. Mater. Sci.* **10** (1975) 1527.
16. A. G. EVANS, "Fracture Toughness: The Role of Indentation Techniques", in "Fracture Mechanics Applied to Brittle Materials", (ASTM STP 678, ASTM, Philadelphia, 1979) p. 112.
17. N. H. MACMILLAN, *Amer. Ceram. Soc. Bull.* **59** (1980) 697.
18. E. RABINOWICZ, "Friction and Wear of Materials", (Wiley, New York, 1965).
19. K. MIYOSHI and D. H. BUCKLEY, "Considerations in Friction and Wear", in "Tribology in the '80s", Vol. 1, (NASA CP-2300, NASA, Washington, DC, 1984) p. 291.
20. O. O. ADEWOYE and T. F. PAGE, *Wear* **70** (1981) 37.
21. D. W. RICHERSON, L. J. LINDBERG, W. D. CARRUTHERS and J. DAHN, *Ceram. Eng. Sci. Proc.* **2** (1981) 578.
22. J. R. SMYTH and D. W. RICHERSON, *ibid.* **4** (1983) 663.
23. M. A. MOORE and F. S. KING, *Wear* **60** (1980) 123.
24. M. B. PETERSON and S. F. MURRAY, *Metals Eng. Quart.* **7**(2) (1967) 22.
25. E. RABINOWICZ and M. IMAI, "Friction and Wear at Elevated Temperature", Technical Report WADC-TR-59-603 Pt III to Wright Field, The Massachusetts Institute of Technology, Cambridge, Massachusetts, July, 1962.
26. J. D. BYERLEE *J. Appl. Phys.* **38** (1967) 2928.

Received 19 February
and accepted 13 March 1985